L-Proline catalysed synthesis and *in silico* studies of novel α-cyano bis(indolyl)chalcones as potential anti-cancer agents†

Monika Malik,[ab] Nandini Roy, [ID][a] Asha Parveen Sakkarai Mohamed,[b] Humphrey Lotana,[b] Kavita Shah*[b] and Dalip Kumar [ID] *[a]

A diverse range of α-cyano bis(indolyl)chalcones (**21a–r**) were synthesized in high yields (90–95%) through the L-proline catalysed reaction of appropriate aldehydes and 3-cyanoacetylindoles. Formation of α-cyano bis(indolyl)chalcones involves readily available starting materials, catalytic L-proline, environmentally benign and metal-free conditions. The prepared eighteen α-cyano bis(indolyl)chalcones **21a–r** were screened against prostate, breast, epithelial cancer cells and found to be non-cytotoxic to normal HEK293 cells. The α-cyano bis(indolyl)chalcones **21a** (3.9 μM), **21c** (7.5 μM), **21i** (2.2 μM) and **21o** (5.9 μM) displayed good cytotoxicity against C4-2 cells, whereas, derivatives **21c** (1.23 μM), **21h** (5.23 μM), and **21l** (2.5 μM) showed selective cytotoxicity against 22Rv1 cells. With broad spectrum of activity (0.98–5.6 μM), the compound **21j** was found to increase the endogenous level of ROS, upregulate the level of p-53 and c-jun besides mitochondrial dysfunction, cause apoptosis.

1. Introduction

The indole motif is a key building block of many naturally occurring and synthetic compounds endowed with different biological activities. Heterocyclic compounds are a significant source of pharmacologically active compounds, and can be obtained from organic synthesis or isolated from natural products.[1] Heterocyclic compounds with one or more nitrogen, oxygen or sulphur, besides at least one carbon in the ring could be used as potential hydrogen bond donors and acceptors. With wider presence among a large number of heterocyclic compounds endowed with interesting medicinal properties, indole and derived compounds have been pursued with greater interest.[2] Particular attention has been paid to bisindole containing compounds which are known to exhibit interesting anticancer activities by affecting numerous biological targets.[3] Additionally, bisindole alkaloids, isolated from marine sources, continue to inspire for the development of novel anticancer agents. Most of the bisindole alkaloids possess two indole units connecting either through a linear or heterocyclic ring spacer as shown in Fig. 1. Isolated from marine sponges *Topsentia genitrix* and *Spongosorites*, bisindole alkaloids, Topsentin (**1**) and Nortopsentin (**2**) with an imidazole linker, have been reported to

display potent cytotoxicity against diverse cancers.[4] Another emerging class of marine alkaloid, Dragmacidin B (**3**) with a piperazine linker, was isolated from the deep-water marine sponge *Hexadella* sp. and found to display good anticancer activity (IC$_{50}$ = 15 μg mL^{-1}, P388; 1–10 μg mL^{-1}, A-549, HCT-8 and MDA-MB-231).[5]

Despite the interesting anticancer activity exerted by bisindole alkaloids, in the recent past, researchers have identified several synthetic analogues of bisindole alkaloids with improved anticancer properties.[6,7] Kumar *et al.* identified bis(indolyl)-1,3,4-oxadiazoles (**4**) as apoptosis inducing cytotoxic agents (IC$_{50}$ = 20 nM; HeLa).[8] Several synthetic analogues

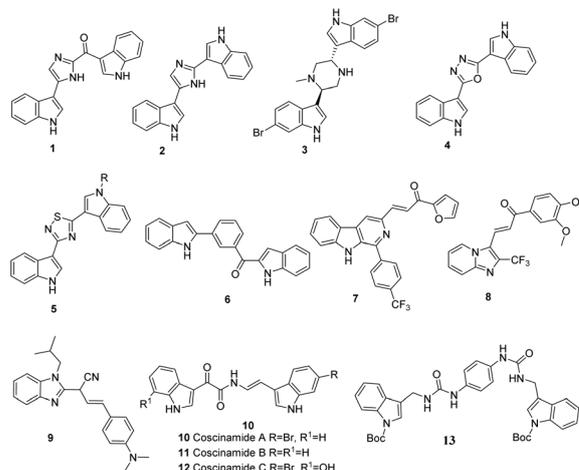*aDepartment of Chemistry, Birla Institute of Technology and Science, Pilani 333 031, India. E-mail: dalipk@pilani.bits-pilani.ac.in*

bDepartment of Chemistry, Purdue University Center for Cancer Research, Purdue University, West Lafayette, IN 47907, USA. E-mail: shah23@purdue.edu

† Electronic supplementary information (ESI) available. See DOI: https://doi.org/10.1039/d4ra06796g

Fig. 1 Indole analogues as anticancer agents.

of bisindole alkaloids with variety of cyclic spacers such as thiazole (**5**), have been reported for their cytotoxic properties (Fig. 1).[9] The inhibition of tubulin polymerization is a well-established strategy for anticancer drug development, as microtubules play an essential role in cellular processes such as mitosis, intracellular transport, and cell motility.[10] Tubulin targeting substances are broadly categorized into microtubule stabilizing (taxanes, epothilones and discodermolide) and destabilizing (colchicine, vinca alkaloids, and CA-4P) agents. Microtubules targeting agents (MTAs) (**6**) that bind to the colchicine binding site (also called CBSI) have the potential to overcome the drawbacks associated with taxanes and vinca alkaloids, owing to their structural simplicity, non-substrate nature for the multidrug resistance protein 1 (P-glycoprotein) and reasonable physicochemical properties.[11,12]

Kamal and Nagesh group explored chalcone linked β-carboline hybrids (**7**) as anti-topoisomerase-I, DNA-interactive, and apoptosis inducing anticancer agents.[13] The α-methylated chalcones (**8**) were prepared by Kamal and Pal-Bhadra group showed 10-folds enhanced activity when compared to their parent derivatives.[14] Natural and synthetic chalcones have been reported to show diverse biological activities such as antiinflammatory,[15] antimalarial,[16] antiviral, antifungal, antibacterial[17] and anticancer.[17] The *N*,*N*-dimethylamino substituted acrylonitrile bearing *N*-isobutyl and cyano substituents placed on the benzimidazole nuclei (**9**), showed strong and selective antiproliferative activity in submicromolar range of inhibitory concentrations (IC$_{50}$ = 0.2–0.6 μM), while being significantly less toxic than reference systems docetaxel and staurosporine, thus promoting them as lead compounds.[18] Coscinamides A–C (**10–12**) with a linear α-keto enamide spacer from the extract of marine sponge *Coscinoderma* sp., were reported to exhibit antitumor activity against human prostate cancer cell line (IC$_{50}$ = 7.6 μg mL^{-1}).[19] Isolated from a red alga *Chondria* sp. two cytotoxic bis-indole amides, chondriamides A–B, were found to be cytotoxic against KB and LOVO cell lines (IC$_{50}$ = 0.5–10 μg mL^{-1}).[20] In 2023, Jan *et al.* conducted a study focused on synthesizing novel bis-indole analogues containing a phenyl linker derived from indole phytoalexins. The synthesis involved the reaction of [1-(*tert*-butoxycarbonyl)indol-3-yl]methyl-isothiocyanate with *p*-phenylenediamine to obtain the target bis-indole thiourea (**13**) linked with a phenyl linker.[7] Literature reports show that the indole scaffold frequently encounters in anticancer drug discovery research as illustrated in Fig. 1. On the other hand, the α,β-unsaturated ketones also known as chalcones are reported to play a vital role in the identification of bioactive molecules. Indolyl chalcones (**14**) as potential cytotoxic agents.[21] Boumendjel *et al.* first reported that α-substituted chalcones are more potent than their unsubstituted analogs.[22a] Li and Huang group reported (**15**), exhibited most potent activity, with IC$_{50}$ values of 3–9 nM and also displayed excellent tubulin polymerization inhibitory activity with an IC$_{50}$ of 2.68 μM.[22b]

Inspired from the interesting anticancer activities of naturally occurring bis-indoles with linear chain spacers, Kumar *et al.* report ed bis(indolyl)hydrazide-hydrazones (**16**) as potent cytotoxic agents (IC$_{50}$ = 1 μM; MDA-MB-231).[23] Over a period of

time, several chalcones have been reported with structural modifications around the basic enone template.[14] Liu X. *et al.* reported the synthesis of hybrid molecules containing indole and 3,4,5-trimethoxy-phenyl moieties as tubulin targeting agents. Among them, a fluorine-containing derivative (**17**) (Fig. 2) exhibited significant inhibitory activity toward HCT116 and CT26 cells.[24a] Additionally, the presence of a α-cyano moiety in enone framework likely to plays an important role in view of its several advantageous properties, including enhanced binding affinity, improved pharmacokinetic profiles and reduced drug resistance.[25,26a] *Trans*-indol-3-ylacrylamide (**18**) exhibited antiproliferative activity, with an IC$_{50}$ value of 5 μM in Huh7 cells.[24b] In 2011, Venkatanarayana and Dubey reported triphenylphosphine (40 mol%) promoted synthesis of α-cyano bis(indolyl)chalcones involving the reaction of indole-3-carboxaldehydes with 3-cyanoacetylindole.[26b] Cluskey *et al.* reported a library of substituted acrylonitriles *via* piperidine catalysed reaction of 3-oxo-3-(1*H*-pyrrol-2-yl)propanenitrile with various substituted benzaldehydes at 70 °C.[26c] In 2014, Kumar *et al.* prepared different α-cyano bis(indolyl)chalcones by employing microwave-assisted reaction of indole-3-carboxaldehyde with 3-cyanoacetylindole in presence of piperidine (0.2 mL for 1 mmol) at 80 °C. Some of the α-cyano bis(indolyl) chalcones exhibited cytotoxicity against lung cancer cells and their preliminary mechanism of action studies indicated weak enhancement of tubulin polymerization.[26d] In our current work, the L-proline catalysed economical and practical synthesis of α-cyano bis(indolyl)chalcones is advantageous due to high product yields, easy isolation and ambient reaction conditions. The heterocyclic pharmacophores in medicinal chemistry plays a crucial role in developing potent moieties towards successful cancer drug design. Among them all bisindole derivatives are the leading structural fragments which play an important role in synthetic and medicinal chemistry as well as various other fields. With the observed side effects and high resistance rate against available drugs; identification of new and potent chemical entities is desirable to tackle the increasing disease problem.[9,27] In efforts to develop eco-friendly protocol and identify potent and selective tubulin interacting agents, in present work, we prepared a new set of α-cyano bis(indolyl)chalcones with improved colchicine binding site affinity, *via* proline catalysed reaction of readily available indole-3-carboxaldehyde with 3-cyanoketones in ethanol at room temperature.
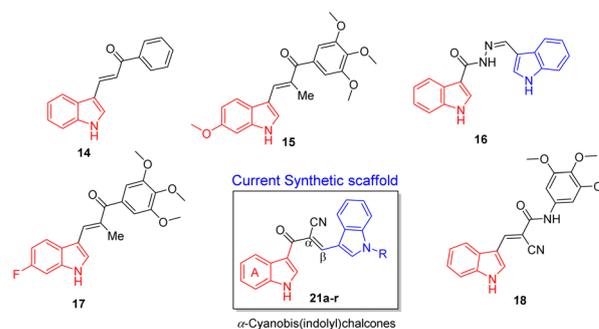

Fig. 2 Rational design of **21**.

2. Results and discussion

2.1 Synthesis

Synthesis of α-cyano bis(indolyl)chalcone (**21a**) involves the reaction of 3-cyanoacetyl indole (**19a**) with *N*-methyl indole-3-carboxaldehyde **20a** in presence of a base as described in Table 1. Initially, the reaction of **19a** with **20a** in presence of either piperidine or triethylamine resulted in lower product yield (Table 1, entries 1 and 2). Next, with the use of KOH as a base at 25 °C produced the expected α-cyano bis(indolyl) chalcone **21a** in 80% yield (Table 1, entry 3). With the increase in reaction time from 2.5 h to 3 h, the product yield was increased to 93% (Table 1, entry 4). When a neat mixture of 3-cyanoacetylindole **19a** and *N*-ethylindole-3-carboxaldehyde (**20a**) in the presence of KOH was grinded at room temperature for 0.5 h, bis-indole **21a** was formed in 88% yield (Table 1, entry 5). No product was obtained when the same reaction was performed in absence of base (Table 1, entry 6). The use of L-tryptophan as a catalyst at 25 °C produced the expected α-cyano bis(indolyl)chalcone **21a** in 42% yield (Table 1, entry 7).

In the recent past, the natural and inexpensive L-proline has been widely used as a prominent organocatalyst for carbon–carbon bond formation in various organic transformations.[26a] In view of success of proline catalysed transformations along with its inexpensive and environmentally benign nature, next we performed the reaction of 3-cyanoacetylindole **19a** and *N*-ethyl indole-3-carboxaldehyde **20a** in the presence of readily available and metal-free catalytic L-proline, in ethanol at 25 °C, to obtain **21a** in 95% yield (Table 1, entry 9) as illustrated in Scheme 1. Using a mixture of solvents (EtOH : H₂O), desired product **21a** obtained in 78% yield (Table 1, entry 10). However, in absence of L-proline, the reaction was failed to produce **21a** (Table 1, entry 11). The structure of **21a** was confirmed by the
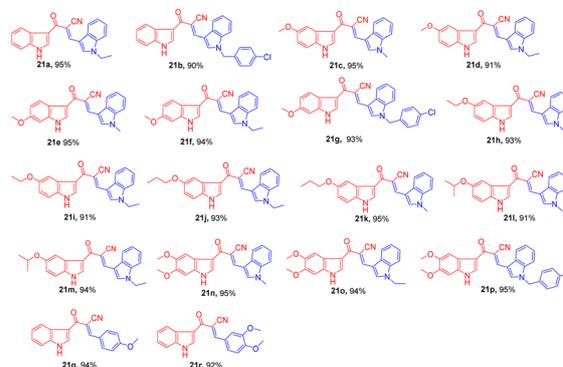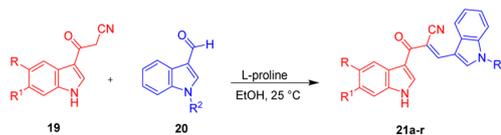
Scheme 1 Synthesized α-cyano bis(indolyl)chalcones **21a–r**.
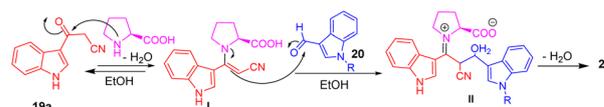
Scheme 2 Plausible mechanistic pathway for the formation of α-cyano bis(indolyl)chalcones.

NMR (^{1}H & ^{13}C) and mass analysis. The proton NMR of **21a** displayed characteristic singlets at 8.50 ppm (alkenyl proton, =CH), 4.44 ppm (CH₂) while CH₃ protons resonated at 1.46 ppm.

In ^{13}C NMR spectrum signals due to carbonyl, nitrile carbon, alkenyl (=CH), CH₃ and CH₂ carbons were observed at about 181.26, 121.07, 144.96, 42.18 and 15.60 ppm, respectively. In IR spectra, a characteristic sharp peak at ~2200 cm^{-1} was observed due to the presence of a nitrile functional group. Mass spectrum of **21a** showed a peak at m/z 340.1595 in agreement with the calculated mass at m/z 340.1405 $(M + H)^+$ for $C_{22}H_{17}N_3O$. Similarly, using the optimized reaction conditions, compounds **21b–r** were prepared in high yields (90–95%) and characterized the products by their NMR and mass spectral data (Scheme 1).

The formation of **21** may be rationalized by the *in situ* generation of enamine intermediate **I** by the condensation of 3-cyanoacetyl-indole **19a** and L-proline. Further, the nucleophilic addition of enamine **I** to the carbonyl group of indole-3-carboxaldehyde (**20**) and followed by dehydration is likely to produce **21** as illustrated in Scheme 2.

2.2 Biological evaluation

2.2.1 Anticancer activity. The cytotoxicity of the synthesized α-cyano bis(indolyl)chalcones derivatives **21a–r** were evaluated against five human cancer cell lines; prostate (C4-2, PC3 and 22Rv1), breast (MCF7), epithelial cancer (MIAPACA) and normal human kidney (HEK293) cell lines by using MTT assay. The anticancer activity is expressed in terms of IC₅₀ values for inhibition of tumor cell growth as provided in

Table 1 Optimization of reaction conditions for **21a**^{a,b}

Entry	Solvent	Base	Temp.	Time (h)	Yield^b (%)
1	EtOH	Piperidine	25 °C	2.5	48
2	EtOH	Et₃N	25 °C	2.5	45
3	EtOH	KOH	25 °C	2.5	80
4	EtOH	KOH	25 °C	3.0	93
5	—	KOH	25 °C	0.5	88^c
6	EtOH	—	25 °C	2.5	NR^d
7	EtOH	L-Tryptophan	25 °C	2.5	42
8	EtOH	L-Proline	25 °C	2.5	67
9	**EtOH**	**L-Proline**	**25°C**	**5.5**	**95**
10	EtOH : H₂O (1 : 1)	L-Proline	25 °C	5.5	78
11	**EtOH**	—	**25°C**	**5.5**	NR^d

^{a} Reagents and conditions: **19a** (1.0 mmol, 1.0 equiv.), **20a** (1.0 equiv.), L-proline or L-tryptophan (0.1 equiv.), EtOH (3 mL) at 25 °C. ^{b} Isolated yield. ^{c} Grinding. ^{d} NR; no reaction.

Table 2. A structure–activity relationship (SAR) study was conducted by synthesizing a diverse set of α-cyano bis(indolyl) chalcones with various substituents on both indole rings (Fig. 3).

Most of the synthesized compounds are not inhibiting the normal cells (HEK293). Initial bis-indole **21a** was found to be selectively cytotoxic against C4-2 (IC$_{50}$ = 3.9 μM). Next, protection of indole-NH with *p*-chlorobenzyl moiety produced **21b** with moderate activity. Incorporation of a C5-methoxy group in indole moiety led to compounds **21c** and **21d**. Particularly, compound **21c** with 5-methoxyindole and *N*-methylated indole displayed selective cytotoxicity against 22Rv1 (1.23 μM). With the change in position of methoxy group in indole ring from C-5 to C-6 and protection of indole NH with *p*-chlorobenzyl group led to compounds **21e**, **21f** and **21g** with reduced activity. To optimize the size of C5-alkoxy group, ethoxy and propyloxy derivatives **21h**, **21i** and **21j** were prepared with significantly enhanced cytotoxicity against the tested cancer cells. By the introduction of 5-isopropyloxy group led to **21l** with improved selectivity against prostate cancer cells (2.5 μM, 22Rv1 cells). The presence of an additional methoxy group in indole ring and protection of indole NH as *N*-Me/*N*-Et (compounds **21n** and **21o** with 5,6-dimethoxyindole moiety) improved the selectivity against prostate cancer cell lines. The protection of indole nitrogen with *p*-chlorobenzyl moiety (compounds **21p**) or replacement of the indole ring with a phenyl group (compounds **21q** and **21r**) or was found to be detrimental for the activity. These activity results suggest that both the indole rings are necessary for the potency of α-cyano bis(indolyl)chalcones. Protection of second indole ring as *N*-Et (**21j**) instead of *N*-Me (**21k**) or *N*-chlorobenzyl (**21b**) is also beneficial for the activity. Particularly, **21j** with C-5 propyloxy substituent and *N*-ethyl-indole was found to be the best compound of series with an IC$_{50}$ value of 0.98 μM against C4-2 (prostate) cancer cells.

2.2.2 Ethidium bromide (EB)/acridine orange (AO) assay for simultaneously ascertaining cell viability and death. Our
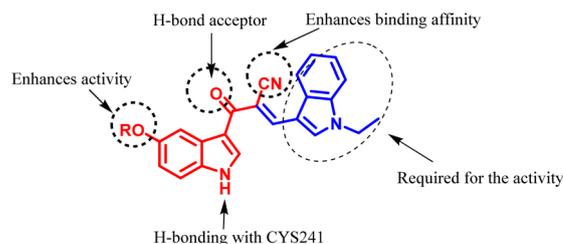

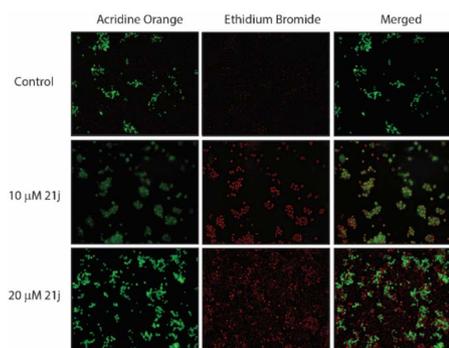Fig. 3 SAR for the α-cyano bis(indolyl)chalcones (**21a–r**).

Fig. 4 Fluorescent AO images of C4-2 cells treated with DMSO or **21j** for 48 h, followed by AO–EB staining. Control cells are viable as they show green fluorescence. Both 10 and 20 μM concentrations of **21j** induced substantial apoptosis as visualized by the red fluorescence.

results showed that **21j** was the most effective compound across all cancer cell lines tested, with no notable impact on non-cancerous HEK293 cells, prompting us to investigate the mechanism of cell death. We initially employed EB/AO staining to ascertain the percentage of dead and live cells. AO stains both live and dead cells. In contrast, ethidium bromide (EB) stains only dead cells. Treatment of compound **21j** in C4-2 cells for 48 h caused robust cell death as indicated by enhanced red fluorescence as compared to control DMSO-treated cells (Fig. 4).

2.2.3 21j triggers mitochondrial depolarization in C4-2 cells. Mitochondria are known to generate significant amount of ROS from at least ten different sites, which in turn increases intracellular oxidative stress. As oxidative stress triggers mitochondrial damage, we investigated whether **21j** exposure could cause mitochondrial depolarization. C4-2 cells were treated with 10 μM or 20 μM of compound **21j** for 48 h, both of which induced significant mitochondrial depolarization, thereby confirming that **21j** cytotoxicity at least partly arises due to mitochondrial dysfunction (Fig. 5).

2.2.4 Induces reactive oxygen species (ROS) accumulation. Increased oxidative stress induces cell death. Therefore, we examined whether compound **21j** promotes ROS using DCFDA staining in C4-2 cells. Both 10 μM and 20 μM concentrations of **21j** induced robust increase in ROS levels (Fig. 6). These results confirm that **21j** induces cytotoxicity at least in part by increasing oxidative stress.

2.2.5 Induces tubulin depolymerization. Low levels of ROS levels promote cytoskeleton polymerization, but high levels of

Table 2 IC$_{50}$ (μM) values of α-cyano bis(indolyl)chalcones (**21a–r**)

Compd	MCF7	PC3	C4-2	22Rv1	MIAPACA	HEK293
21a	10.2	13	**3.9**	>40	>40	>40
21b	**6.9**	10.6	13.5	21.5	**4.9**	40
21c	25.3	15.45	**7.5**	**1.23**	**4.5**	>40
21d	10.9	>40	8	25	15.5	39.2
21e	12.47	**7.61**	15.7	28	>40	>40
21f	37	24	12.5	>40	>40	40
21g	10.5	14.3	13.3	34	**7.9**	>40
21h	16.75	27.3	10	**5.23**	**1.35**	40
21i	**7.38**	**2.63**	**2.2**	8.9	5.8	**>40**
21j	**1.2**	**5.6**	**0.98**	**2.9**	5.3	**>40**
21k	18.6	16.1	13.8	28	28.9	39.8
21l	7.95	4.6	26.4	**2.5**	37.6	37.9
21m	**2.98**	11.7	17.6	16.4	**1.6**	>40
21n	**5.61**	**7.1**	**1.02**	20.5	15.6	>40
21o	31.5	19	**5.9**	26	12.95	>40
21p	>40	>40	31	>40	>40	>40
21q	25	37	>40	28	15.4	>40
21r	>40	25	>40	34	37	31
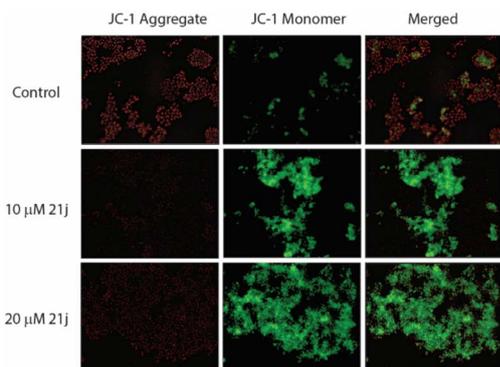
Fig. 5 **21j** induces mitochondrial depolarization in C4-2 cells. Cells were treated with either DMSO or **21j** at concentrations of 10 μM and 20 μM for 48 h, and then stained with JC-1. Images were captured using a fluorescence microscope (Keyence) with FITC (green) and TRITC (red) channels at a 20× magnification objective.
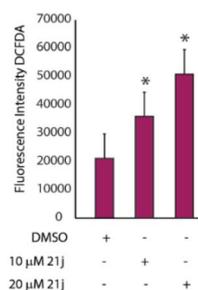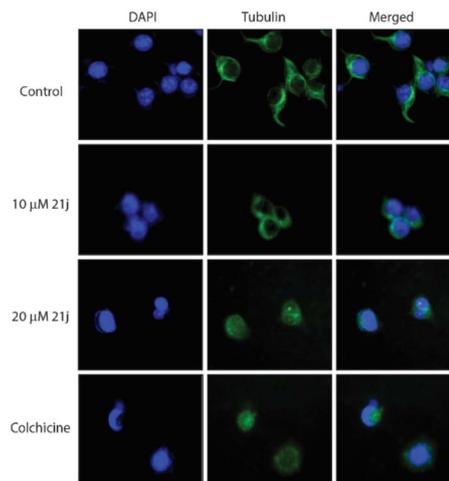

Fig. 6 **21j** raises the levels of ROS in C4-2 cells. C4-2 cells were treated with either 10 μM and 20 μM of **21j** for 48 h. Following treatments, they were stained using H2-DCFDA. The bar graph depicts relative ROS levels (green signal) using control DMSO, 10 μM **21j**-treated and 20 μM **21j**-treated cells. Data analysis was performed using three independent replicates, and statistical significance between DMSO (control), 10 and 20 μM **21j**-treated cells were performed using Student's T-test. *$P < 0.05$.

Fig. 7 **21j** increases tubulin depolymerization in C4-2 cells. C4-2 cells were exposed to either DMSO (negative control) or **21j** at two concentrations (10 μM and 20 μM) for 48 h and stained with tubulin antibody. Colchicine was used as the positive control. Photographs were taken in FITC (green) and DAPI (blue) channels at 20× objective with the fluorescence microscope (Keyence).
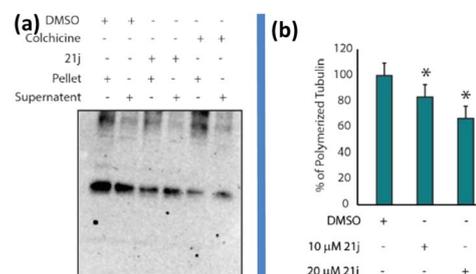
Fig. 8 Tubulin polymerization is increased by **21j** in C4-2 cells. (a) C4-2 cells were exposed to colchicine (100 nM) or compound **21j** (20 μM) for 24 h. DMSO was used as a negative control. Following cell lysis in hypotonic buffer, pellet and supernatant were separated using ultra-centrifugation. Equal amounts of proteins were loaded in each lane. (b) Data analysis was performed using 3 independent replicates, and statistical significance between DMSO (control), colchicine, and **21j**-treated cells was determined using Student's T-test. *$P < 0.05$.

ROS levels inhibit microtubule polymerization. As **21j** increases ROS levels, we examined whether **21j** has an effect on tubulin polymerization in C4-2 cells. Accordingly, C4-2 cells were exposed to **21j** for 48 h and then analysed using β-tubulin antibody. These data showed significant loss of tubulin assembly in **21j**-exposed group. These cells resembled colchicine-treated cells, which is a highly potent tubulin polymerization inhibitor (Fig. 7).

To further validate a potential impact of **21j** on tubulin dynamics, we measured the relative concentrations of polymerized *versus* depolymerized tubulin in control and **21j**-treated C4-2 cells. As a positive control, colchicine was employed. While colchicine treatment significantly decreased the levels of polymerized tubulin by ∼30% as compared to control. **21j** treatment also resulted in ∼20% less polymerized tubulin. These results suggest that at least some percentage of **21j**'s anti-cancer effect stems from its tubulin-depolymerizing activity (Fig. 8).

2.2.6 21j reduces the number and size of colonies. Clonogenic assay is an *in vitro* cell based technique that is often used to determine the tumorigenic potential of cells *in vivo*. Therefore, we determined the effect of **21j** on colony forming ability of C4-2 cells. **21j** treatment significantly inhibited the number and size of colonies as compared to the control group (Fig. 9) indicating that **21j** should serve as an effective anti-cancer agent.

2.3 Molecular docking studies

Tubulin–colchicine complex (PDB code: 1SA0) structure was provided by the Protein Data Bank (https://www.rcsb.org/).[28] To explore the potential interactions between tubulin and α-cyano bis(indolyl)chalcones, including compound **21j**, we compared their orientations with the reference drug colchicine. To better understand the potency of **21j**, we examined its interaction with the tubulin crystal structure (PDB code: 1SA0) using AutoDock 1.5.6 software (The Scripps Research
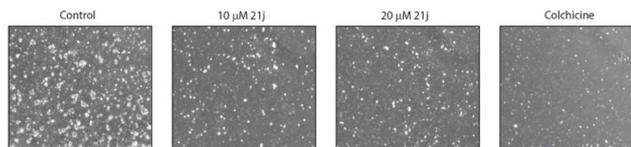
Fig. 9 Compound **21j** inhibits colony formation in C4-2 cells. An equal number of cells (1000 cells per well) were plated in a 6-well plate. They were treated with 0.05% DMSO (control) or compound **21j** at 10 μM or 20 μM. 200 nM colchicine was used as a positive control. After 10 days cells were fixed and photographed.

Institute, USA). The X-ray crystallographic structure of the tubulin–colchicine complex reveals a crucial hydrogen bonding interaction with CYS241, along with additional hydrophobic interactions. The selected pose of the **21j** out of eight poses that showed similarity to the binding mode of DAMA colchicine is considered the best pose with binding energy is -7.7 kcal mol^{-1} (Fig. 10). As shown in Fig. 10, C$_5$-propyloxy and NH moieties of indole in **21j** form hydrogen bonding interactions with CYS241 and LEU255, respectively, in addition to hydrophobic interactions (ALA250, ALA354, LEU248, ALA316, LYS352).

Molecular docking results further highlight that **21j** as a novel tubulin polymerization inhibitor that displayed interactions in the colchicine binding site of the tubulin. The structures were visualised and analysed in Discovery studio 2021 software (Fig. 10).

2.4 Molecular dynamics simulation studies

To further elucidate the procedural binding mode of **21j** and tubulin, a 100 ns molecular dynamics (MD) study was performed based on the docked conformation of **21j** with tubulin (PDB:1SA0). Through MD simulations, root mean square deviation (RMSD) plot for the protein–ligand complex **21j**-1SA0 was determined between 6–8 Å and the complex was centred without significant scattering (Fig. 11a). This indicates that the ligand formed a stable binding with protein throughout the simulation. The protein-ligand contact map in Fig. 11c indicated that CYS241, ALA251, ASN258, and LYS352 were highly involved in H-bond formation with the ligand **21j** during the MD simulation. Additionally, the RMSF plot along with the heatmap simulation trajectory point out the stability of the acquired docking model, as illustrated in Fig. 11. Moreover, a 2D diagram of the ligand–protein contacts of **21j**-1SA0 (Fig. S1, ESI†), shows important interactions of **21j** with the protein
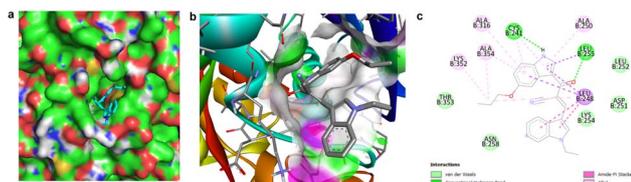
Fig. 10 (a) **21j** in the binding pocket of the protein 1SA0. (b) 3D view of **21j** with β-tubulin. (c) 2D overview of the molecular interactions of **21j** in colchicine binding site of 1SA0.
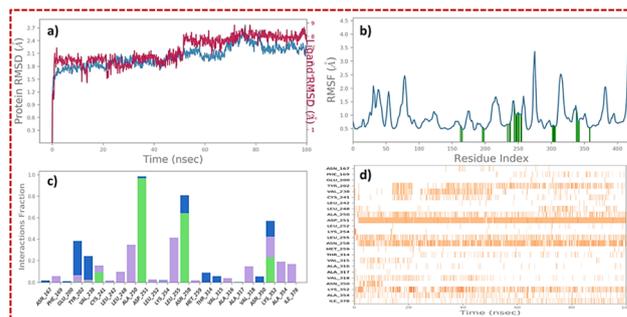
Fig. 11 Statistical analysis of the MD simulation trajectory. (a) RMSD plot showing the ligand-bound state (red) and the Cα atoms of the target protein (blue), illustrating system stability over the 100 ns simulation. (b) RMSF plot of the protein-ligand complex, with green spikes highlighting the ligand binding site residues during the simulation. (c) Protein–ligand contact mapping in a bar plot, indicating the frequency and duration of interactions of the protein with the ligand **21j**. (d) Heatmap illustrating the consistency and strength of interactions between the protein and ligand over the simulation trajectory.

residues. A detailed description of the MD study of the complex is given in the ESI.†

2.5 In silico ADMET evaluation of α-cyano bis(indolyl) chalcone 21a–r

As a result, numerous in silico models have been developed to predict chemical ADMET (Absorption, Distribution,
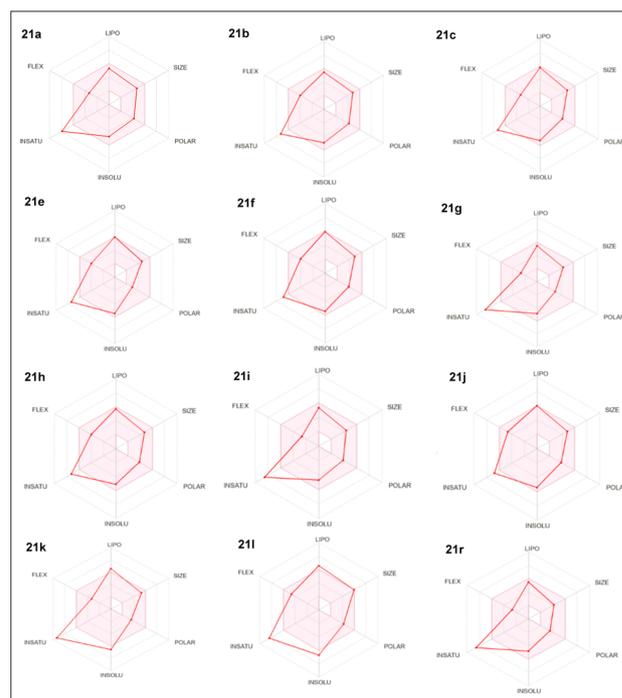
Fig. 12 Oral bioavailability radar charts for the studied potent compounds **21a–r**. In bioavailability radar, the pink area represents the optimal range for each physicochemical property of oral bioavailability (LIPO-lipophilicity, SIZE-size, POLAR-polarity, INSOLU-solubility, INSATU-saturation and FLEX-flexibility), while the red lines represent compounds: **21a–r**.

Table 3 Physicochemical properties of **21a–r**

Compd	MW^a (g mol^{-1})	$C \log P_{o/w}{}^b$	nHBA^c	nHBD^d	nRB^e	TPSA (Å^2)^f	Log S^g	Druglikeness
21a	339.39	3.70	2	1	4	61.58	−4.97	Yes
21b	435.90	5.16	2	1	5	61.58	−6.58	Yes
21c	355.39	2.91	3	1	4	70.81	−4.67	Yes
21d	369.42	3.17	3	1	5	70.81	−4.86	Yes
21e	355.29	3.36	3	1	4	70.81	−4.67	Yes
21f	369.42	3.68	3	1	5	70.81	−4.86	Yes
21g	465.93	5.14	3	1	6	70.81	−6.65	Yes
21h	399.44	3.68	4	1	6	80.04	−4.93	Yes
21i	383.44	4.03	3	1	6	70.81	−5.09	Yes
21j	**397.47**	**4.40**	**3**	**1**	7	**70.81**	**−5.43**	**Yes**
21k	383.44	3.37	3	1	6	70.81	−5.24	Yes
21l	354.40	3.92	2	1	4	47.02	−4.86	Yes
21r	332.35	3.18	4	1	5	75.11	−4.34	Yes

^{a} Molecular weight. ^{b} Lipophilicity. ^{c} No. of H-bond acceptors. ^{d} No. of H-bond donor. ^{e} No. of rotatable bonds. ^{f} Topological surface area. ^{g} water solubility.

Table 4 Selected pharmacokinetic parameters of **21a–r**

Compd	GI absorption	BBB permeant	Log K_p (cm s^{-1})	CYP1A2	CYP2C19	CYP2C9	CYP2D6	CYP3A4
21a	Low	No	−5.07	No	Yes	Yes	No	Yes
21b	High	Yes	−5.45	Yes	Yes	Yes	No	Yes
21c	High	Yes	−5.54	Yes	Yes	Yes	No	Yes
21d	High	Yes	−5.45	Yes	Yes	Yes	No	Yes
21e	High	No	−5.25	Yes	Yes	Yes	No	Yes
21f	High	No	−5.25	Yes	Yes	Yes	No	Yes
21g	High	No	−5.25	Yes	Yes	Yes	No	Yes
21h	High	No	−5.38	Yes	Yes	Yes	No	Yes
21i	High	No	−5.47	Yes	Yes	Yes	No	Yes
21j	**High**	**No**	**−5.18**	**Yes**	**Yes**	**Yes**	**No**	**Yes**
21k	High	Yes	−5.07	Yes	Yes	Yes	No	Yes
21l	High	No	−5.25	Yes	Yes	Yes	No	Yes
21r	High	Yes	−5.45	Yes	Yes	Yes	No	Yes

Metabolism, Excretion, and Toxicity) properties and it has become advantageous as it reveals a pharmacokinetics-related failure of drugs before proceeding to the clinical phase.[29a] Lipophilicity is generally considered a key determinant of permeability across tissue membranes, while water solubility is another physicochemical property that determines a drug's ADMET behaviours. Here, we evaluate the ADME properties of the synthesized compounds by using *in silico* SwissADME server to see the pharmacokinetic properties such as lipophilicity, water-solubility, drug-likeness, medicinal chemistry of the compounds (Fig. 12).[29b]

Orally administered drugs typically exhibit high lipophilicity, which facilitates their absorption through the intestinal lining, penetration of target cell membranes, and transport within the bloodstream. There is a direct relationship between the log P value and lipophilicity, but this negatively correlates with water solubility.[26a] The calculated log P values of test compounds **21a–r** ranges between 3.17 and 5.16. Drug-likeness is established based on chemical structures and physicochemical properties and is a qualitative assessment of oral bioavailability.[30] Moreover, Lipinski's rule states that for an orally active drug, the following conditions must be obeyed: ≤5 H-bond donors, ≤10

H-bond acceptors, a molecular weight ≤500 g mol^{-1}, and a log P ≤ 5.43; a ligand is considered orally inactive if it violates two or more of Lipinski's rules.[31] Considering these criteria, all the compounds **21a–r** meet the requirements for oral bioavailability (Table 3). Moreover, none of the test compounds violated Veber's rule, whose criteria are the presence of rotatable bonds ≤10 and polar surface (TPSA) area ≤140 Å^2.[31] Moreover, evident from the bioavailability score of 0.55, all the selected test compounds **21a–r** are orally suitable.
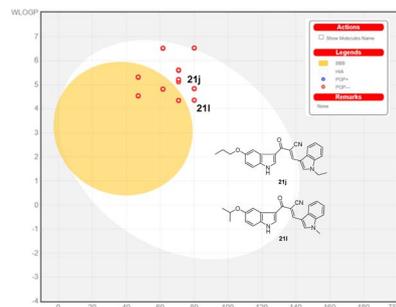

Fig. 13 BOILED-Egg plot for α-cyano bis(indolyl)chalcones **21j**.

Table 5 Physiochemical and ADME parameters

	Toxicity probability of compounds				
Toxicity target	Colchicine	21i	21j	21m	21n
Caco-2 permeability	0.65	0.53	0.53	0.58	0.51
Rat acute toxicity (LD_{50}) mol kg^{-1}	2.37	2.63	2.61	2.56	2.66
Carcinogens	**Non-carcinogens**				
	0.81	0.88	0.91	0.91	0.93
Distribution					
Subcellular localization	**Nucleus**	**Mitochondria**			
P-glycoprotein substrate	0.59	0.52	0.55	0.62	0.60
Absorption	**Log P app, cm s^{-1}**				
Caco-2 permeability	1.17	1.29	1.20	1.29	1.64
Human intestine absorption	0.98 high	1.00 high	1.00 high	1.00 high	1.00 high

Table 4 shows the results of the pharmacokinetics prediction of the potent compounds **21a–r**. As highlighted in the table, the skin permeation values (log K_p in cm s^{-1}) of the test compounds ranged from −5.54 (more permeant) to −5.07 (most permeant). Compounds **21c** and **21j** are the most skin permeant among the prepared compounds; however, the range of values of each test compound suggested that they are permeable compared to the values from the standard ligand. All the test compounds possess high gastrointestinal (GI) absorption potential, and the compounds (**21b, 21c, 21d, 21k** and **21r**) displayed the ability to penetrate the blood–brain barrier (BBB). According to the pharmacokinetic predictions, except for **21a**, all the test compounds were predicted to be inhibitors of CYP1A2, CYP2C19, CYP2C9, CYP2D6, and CYP3A4 (Table 4). Cytochrome P450 (CYP) is an isoenzyme superfamily that catalyzes various biochemical processes in phase I of drug metabolism (Hollenberg, 2002). The inhibition of the five main isoforms CYP1A2, CYP2C19, CYP2C9, CYP2D6, and CYP3A4 from eventually becoming the substrates of medications is a primary cause of pharmacokinetics-related drug interactions.[32]

Moreover, according to Table 4, the bioavailable radar charts (in Fig. 12), and the BOILED-Egg plot in Fig. 13, the investigated compounds were predicted to possess high gastrointestinal tract (GI) absorption and blood–brain barrier (BBB) permeability.

2.6 The BOILED-Egg is of great support for lead optimization

The BOILED-Egg model offers a rapid, and easily reproducible yet statistically robust method for predicting the passive gastrointestinal absorption and brain access of small molecules, which is valuable for drug discovery and development.

Highest probability of absorption by the gastrointestinal tract, while the yellow region (yolk) indicates the highest probability of permeating to the brain.

It's important to note that the yolk and white areas are not mutually exclusive. This means that some compounds can simultaneously have high gastrointestinal absorption and brain permeation. Such compounds are particularly desirable in drug

development as they can effectively reach both systemic circulation and the central nervous system. This dual capability can lead to more efficient treatments for diseases that affect multiple organs, including the brain.

According to the determined parameters related to the absorption of the drug substance, it can be said that the synthesized compounds **21a–r** were characterized by good intestinal absorption (HIA) and bioavailability. Distribution analysis predicted the location of the tested compounds in the mitochondria and did not reveal permeability through the blood–brain barrier (BBB). In addition, the compounds were identified as P-glycoprotein substrates but not inhibitors. *In silico* toxicity and carcinogenicity are assessed and are given in Table 5. Furthermore, the computed rat acute toxicity, that is, LD_{50} in mol kg^{-1} seems to be sufficiently safe in the range 2.23–2.66 mol kg^{-1}. The LD_{50} and other bioactivity score of **21j** is similar to that of the standard colchicine drug shown in Table 5.

3. Conclusions

The high yielding synthesis of indolyl α-cyano bis(indolyl) chalcones was achieved from the L-proline catalysed reaction of appropriate aldehydes with 3-cyanoacetylindoles. Of the prepared eighteen α-cyano bis(indolyl)chalcones, compound **21j** demonstrated remarkable potency against the C4-2 prostate cancer cell line (IC_{50} = 0.9 μM). With broad spectrum of activity (0.98–5.6 μM), the compound **21j** was found to increase the endogenous level of ROS, besides mitochondrial dysfunction, causes apoptosis. Additionally, moderate tubulin activity of **21j** suggest that at least some percentage of **21j**'s anti-cancer effect stems from its tubulin de-polymerization. The molecular docking study of **21j** displayed important interactions in the colchicine binding site of the tubulin which supports its observed tubulin activity.

4. Experimental section

4.1 Chemistry

4.1.1 General methods. All laboratory reagents were purchased from Sigma-Aldrich, BLD Pharma, Alfa Aesar and

Spectrochem India Pvt. Ltd and used without additional purification. Reaction progress was monitored using thin layer chromatography and performed on Merck pre-coated plates (silica gel 60 F254, 0.2 mm). Column chromatographic purification of products was carried out using silica gel (100–200 mesh) and ethyl acetate/hexane mixture was used for elution. NMR (^{1}H and ^{13}C) spectra were recorded at 400 MHz and 100 MHz using CDCl$_3$ and DMSO-d_6 solvents. Chemical shifts are given in ppm relative to the residual solvent peak (^{1}H NMR: CDCl$_3$ δ 7.26; DMSO-d_6 δ 2.50; ^{13}C NMR: CDCl$_3$ δ 77.0; DMSO-d_6 δ 39.52) with multiplicity (s = singlet, d = doublet, t = triplet, q = quartet, m = multiplet), coupling constants (J, in Hz) and integration. Melting points were determined by using E–Z melting point apparatus and are uncorrected. High-resolution mass data (HRMS) were obtained on an Agilent 6545 Q-TOF LC/MS (ESI).

4.1.2 General procedure for the synthesis of 3-cyanoacetyl indoles[33] (19). Methane sulfonyl chloride (0.13 mL, 0.17 mmol) and corresponding indoles (0.20 g, 0.17 mmol) were added to a stirred solution of potassium cyanoacetate (0.42 g, 0.34 mmol) in acetonitrile (3 mL). The resulting solution was stirred at room temperature for 1 h. The progress of the reaction was monitored by TLC. After the consumption of the starting material, contents were allowed to cool and a white solid thus obtained was collected by filtration, washed with methanol and dried to obtain pure products (19a–g) as mentioned below:
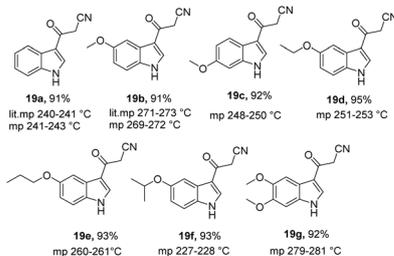
4.1.3 Procedure for the synthesis of 5-alkoxyindoles and 5,6-dimethoxyindole.[34] A mixture of 5-hydroxyindole/5,6-hydroxyindole (0.50 g, 3.8 mmol) and K$_2$CO$_3$ (1.52 g, 11.0 mmol), dissolved in 5 mL ethanol and heated to reflux. The ethyliodide/propylbromide/isopropylbromide (0.77 g, 4.9 mmol) was added and the reaction mixture was allowed to reflux for 1 h and then concentrated the mixture at reduced pressure. Water (20 mL) was added and the aqueous layer was extracted with ethyl acetate (3 × 30 mL). The combined organic layer was dried with MgSO$_4$ and concentrated. The crude product was purified by flash column chromatography using 5% ethyl acetate/hexane (v/v) as eluent.
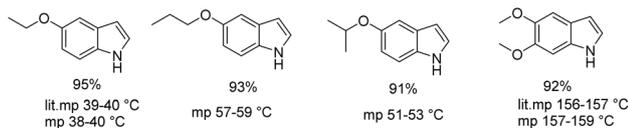
4.1.4 General procedure for the synthesis of indole-3-carboxaldehyde.[26d] A round bottomed flask containing freshly distilled dimethylformamide (DMF) (10 mL) was cooled in an ice–salt bath for about 0.5 h and freshly distilled phosphorus oxychloride was added with stirring to DMF (5 mL) over a period of 0.5 h. A solution of indole (2 g, 85.47 mmol) in DMF (130 mmol) was added to the yellow solution over a period of 1 h. The solution was stirred at 35 °C till it became a yellow paste. At the end of the reaction, 30 g of crushed ice was added to the paste with stirring to obtain a clear cherry-red aqueous solution. To this solution, sodium hydroxide (10 g, 94 mmol) in 100 mL of water was added dropwise with stirring. The resulting suspension was heated rapidly to 90 °C and allowed to cool at room temperature, after which it was placed in refrigerator for overnight. The product was filtered, washed with water (2 × 100 mL) and air dried to afford the pure indole-3-carboxaldehyde in 93% yield, mp 196–197 °C.

4.1.5 Procedure for alkylation of indole-3-carboxaldehydes (20a–c).[35] In a reaction flask, indole-3-carboxaldehyde (1 g, 1.0 equiv.) was dissolved in THF (15 mL), followed by the addition of sodium hydride (0.3 g, 2.5 equiv.) and methyl iodide/ethyl iodide/4-chlorobenzylchloride (3.0 equiv.) at 0 °C to room temperature. Reaction was monitored by the TLC. After the completion of reaction, organic phase was washed twice with aqueous NaHCO$_3$ (50 mL), water and saturated brine (100 mL), and then dried over anhydrous Na$_2$SO$_4$. The solvent was evaporated under vacuum and residue was purified by the column chromatography with ethylacetate and hexane led to pure product (20a–c) as follows: 1-methyl-1H-indole-3-carbaldehyde (20a), 95% yield (mp 68–70 °C), 1-ethyl-1H-indole-3-carbaldehyde (20b), 96% yield, (mp 98–100 °C), 1-(4-chlorobenzyl)-1H-indole-3-carbaldehyde (20c), 98% yield, (mp 117–119 °C).

4.1.6 General procedure for the preparation of α-cyano bis(indolyl)chalcones (21a–r). A mixture containing 3-cyanoacetylindole derivative **19** (0.1 g, 1 mmol) and appropriate aldehyde **20** (0.065 g, 1 mmol) in ethanol (10 mL) was stirred at 25 °C. Catalytic amount of L-proline (10 mol%) was added to reaction mixture and it was stirred for 5 h at 25 °C. The reaction progress was monitored via TLC using a developing solvent system of n-hexane : ethyl acetate. The resulting yellow solid was then recrystallized from ethanol to obtain pure α-cyano bis(indolyl)chalcones **21a–r** in 90–95% yields.

4.1.6.1 (E)-3-(1-Ethyl-1H-indol-3-yl)-2-(1H-indole-3-carbonyl) acrylonitrile (21a). Pale yellow solid, 95% yield, mp 221–222 °C; ^{1}H NMR (400 MHz, DMSO-d_6) δ 12.13 (s, 1H), 8.63 (d, J = 10.5 Hz, 2H), 8.50 (s, 1H), 8.26–8.22 (m, 1H), 7.97 (dt, J = 7.7, 1.0 Hz, 1H), 7.69 (dt, J = 8.2, 0.9 Hz, 1H), 7.59–7.54 (m, 1H), 7.38–7.23 (m, 4H), 4.44 (q, J = 7.2 Hz, 2H), 1.46 (t, J = 7.2 Hz, 3H); ^{13}C NMR (100 MHz, DMSO-d_6) δ 181.26, 144.96, 136.88, 136.34, 134.34, 133.43, 128.50, 126.96, 124.01, 123.74, 122.63, 122.50, 122.07, 121.08, 119.38, 114.81, 112.83, 111.76, 110.12, 102.20, 42.18, 15.60. HRMS (ESI) m/z calcd for C$_{22}$H$_{18}$N$_3$O: 340.1405 (M + H)$^+$, found: 340.1595.

4.1.6.2 3-(1-(4-Chlorobenzyl)-1H-indol-3-yl)-2-(1H-indole-3-carbonyl)acrylonitrile (21b).[26d] Yellow solid, 90% yield, mp 222−225 °C (lit mp 219−221 °C); ^{1}H NMR (400 MHz, DMSO-d_6) δ 12.17 (s, 1H), 8.75 (s, 1H), 8.63 (s, 1H), 8.51 (s, 1H), 8.26 (d, J = 6.5 Hz, 1H), 7.97 (d, J = 7.9 Hz, 1H), 7.59 (d, J = 14.8 Hz, 2H), 7.42 (s, 2H), 7.31 (d, J = 10.0 Hz, 6H), 5.68 (s, 2H); ^{13}C NMR (100

MHz, DMSO-d_6) δ 181.31, 144.92, 136.82, 136.44, 135.84, 134.45, 134.10, 133.09, 129.62, 129.22, 128.41, 126.78, 124.33, 123.95, 122.89, 122.71, 122.01, 120.86, 119.31, 114.75, 112.88, 111.96, 110.51, 102.80, 49.87.

4.1.6.3 2-(5-Methoxy-1H-indole-3-carbonyl)-3-(1-methyl-1H-indol-3-yl)acrylonitrile (21c). Yellow solid, 95% yield, mp 220–221 °C; ^{1}H NMR (400 MHz, DMSO-d_6) δ 12.03 (s, 1H), 8.62 (s, 1H), 8.59 (s, 1H), 8.45 (d, J = 3.3 Hz, 1H), 7.96 (d, J = 7.8 Hz, 1H), 7.77 (d, J = 2.8 Hz, 1H), 7.65 (d, J = 8.3 Hz, 1H), 7.45 (d, J = 8.8 Hz, 1H), 7.40–7.28 (m, 2H), 6.91 (dd, J = 8.7, 2.6 Hz, 1H), 4.01 (s, 3H), 3.81 (s, 3H); ^{13}C NMR (100 MHz, DMSO-d_6) δ 180.90, 156.10, 144.84, 137.34, 134.92, 134.35, 131.66, 128.31, 127.83, 124.03, 122.68, 121.10, 119.11, 114.65, 113.64, 113.59, 111.75, 109.89, 103.84, 101.87, 55.74, 34.22. HRMS (ESI) *m/z* calcd for $C_{22}H_{18}N_3O_2$: 356.1354 (M + H)$^+$, found: 356.1373.

4.1.6.4 3-(1-Ethyl-1H-indol-3-yl)-2-(5-methoxy-1H-indole-3-carbonyl)acrylonitrile (21d). Yellow solid, 91% yield, mp 214–215 °C; ^{1}H NMR (400 MHz, DMSO-d_6) δ 8.63 (d, J = 3.8 Hz, 2H), 8.47 (s, 1H), 7.96 (d, J = 7.7 Hz, 1H), 7.80 (d, J = 2.6 Hz, 1H), 7.67 (d, J = 8.1 Hz, 1H), 7.46 (d, J = 8.8 Hz, 1H), 7.38–7.26 (m, 2H), 6.92 (dd, J = 8.7, 2.6 Hz, 1H), 4.42 (q, J = 7.2 Hz, 2H), 3.82 (s, 3H), 1.45 (t, J = 7.2 Hz, 3H); ^{13}C NMR (100 MHz, DMSO-d_6) δ 180.87, 156.10, 144.81, 136.31, 134.43, 133.30, 131.73, 128.52, 127.88, 123.99, 122.62, 121.18, 119.30, 114.69, 113.62, 113.58, 111.73, 110.12, 103.87, 102.04, 55.73, 42.17, 15.57. HRMS (ESI) *m/z* calcd for $C_{23}H_{20}N_3O_2$: 370.1511 (M + H)$^+$, found: 370.1721.

4.1.6.5 2-(6-Methoxy-1H-indole-3-carbonyl)-3-(1-methyl-1H-indol-3-yl)acrylonitrile (21e). Yellow solid, 95% yield, mp 217–220 °C; ^{1}H NMR (400 MHz, DMSO-d_6) δ 11.92 (s, 1H), 8.59 (d, J = 6.2 Hz, 2H), 8.37 (d, J = 3.1 Hz, 1H), 8.09 (d, J = 8.8 Hz, 1H), 7.96 (d, J = 7.9 Hz, 1H), 7.65 (d, J = 8.1 Hz, 1H), 7.41–7.27 (m, 2H), 7.04 (d, J = 2.4 Hz, 1H), 6.89 (dd, J = 8.8, 2.3 Hz, 1H), 4.00 (s, 3H), 3.82 (s, 3H); ^{13}C NMR (100 MHz, DMSO-d_6) δ ^{13}C NMR (101 MHz, DMSO) δ 180.94, 157.16, 144.81, 137.77, 137.34, 134.95, 133.34, 128.29, 124.02, 122.75, 122.67, 121.08, 120.87, 119.13, 114.92, 112.33, 111.74, 109.88, 101.88, 95.81, 55.74, 34.22. HRMS (ESI) *m/z* calcd for $C_{22}H_{18}N_3O_2$: 356.1354 (M + H)$^+$, found: 356.3691.

4.1.6.6 3-(1-Ethyl-1H-indol-3-yl)-2-(6-methoxy-1H-indole-3-carbonyl)acrylonitrile (21f). Yellow solid, 94% yield, mp 228–230 °C. ^{1}H NMR (400 MHz, DMSO-d_6) δ 11.93 (s, 1H), 8.62 (d, J = 8.3 Hz, 2H), 8.40 (s, 1H), 8.12 (d, J = 8.7 Hz, 1H), 7.95 (d, J = 7.8 Hz, 1H), 7.67 (d, J = 8.2 Hz, 1H), 7.35 (t, J = 7.5 Hz, 1H), 7.28 (t, J = 7.4 Hz, 1H), 7.05 (s, 1H), 6.90 (d, J = 11.1 Hz, 1H), 4.41 (q, J = 7.3 Hz, 2H), 3.82 (s, 3H), 1.45 (t, J = 7.2 Hz, 3H); ^{13}C NMR (100 MHz, DMSO-d_6) δ 180.92, 157.17, 144.79, 137.80, 136.31, 133.34, 128.51, 123.98, 122.78, 122.61, 121.15, 120.91, 119.32, 114.96, 112.31, 111.72, 110.12, 102.05, 95.81, 55.73, 42.16, 15.56. HRMS (ESI) *m/z* calcd for $C_{23}H_{20}N_3O_2$: 370.1511 (M + H)$^+$, found: 370.1538.

4.1.6.7 3-(1-(4-Chlorobenzyl)-1H-indol-3-yl)-2-(6-methoxy-1H-indole-3-carbonyl)acrylonitrile (21g). Yellowish solid, 93% yield, mp 215–217 °C.[36] ^{1}H NMR (400 MHz DMSO-d_6) δ 12.07 (s, 1H), 8.74 (s, 1H), 8.63 (s, 1H), 8.48 (s, 1H), 7.97 (d, J = 7.8 Hz, 1H), 7.80 (s, 1H), 7.61 (d, J = 7.9 Hz, 1H), 7.45 (m, J = 17.1, 8.4 Hz, 3H), 7.31 (m, J = 15.3, 7.8 Hz, 4H), 6.93 (d, J = 9.0 Hz, 1H), 5.68 (s, 2H), 3.81 (s, 3H); ^{13}C NMR (100 MHz, DMSO-d_6) δ 180.91,

156.15, 144.65, 136.52, 136.16, 134.61, 133.96, 133.01, 131.72, 129.67, 129.26, 128.56, 127.84, 124.20, 122.74, 120.88, 119.39, 114.64, 113.67, 113.61, 112.06, 110.57, 103.87, 103.01, 55.74, 49.80. HRMS (ESI) *m/z* calcd for $C_{28}H_{21}ClN_3O_2$: 466.1578 (M + H)$^+$, found: 466.1525.

4.1.6.8 2-(5-Ethoxy-1H-indole-3-carbonyl)-3-(1-methyl-1H-indol-3-yl)acrylonitrile (21h). Yellow solid, 93% yield, mp 217–220 °C. ^{1}H NMR (400 MHz, DMSO-d_6) δ 12.02 (s, 1H), 8.61 (s, 1H), 8.57 (s, 1H), 8.45 (s, 1H), 7.94 (d, J = 7.7 Hz, 1H), 7.78 (d, J = 2.6 Hz, 1H), 7.62 (d, J = 8.1 Hz, 1H), 7.45 (d, J = 8.8 Hz, 1H), 7.29 (t, J = 7.6 Hz, 1H), 7.35 (t, J = 6.9 Hz, 1H), 6.90 (dd, J = 8.8, 2.6 Hz, 1H), 4.06 (q, J = 7.0 Hz, 2H), 3.99 (s, 3H), 1.37 (t, J = 7.0 Hz, 3H); ^{13}C NMR (100 MHz, DMSO-d_6) δ 180.79, 155.31, 144.76, 137.31, 134.84, 134.32, 131.65, 128.33, 127.89, 123.97, 122.62, 121.16, 119.08, 114.69, 114.05, 113.54, 111.69, 109.92, 104.72, 101.88, 63.75, 34.18, 15.31. HRMS (ESI) *m/z* calcd for $C_{23}H_{20}N_3O_2$: 370.1511 (M + H)$^+$, found: 370.1722.

4.1.6.9 2-(5-Ethoxy-1H-indole-3-carbonyl)-3-(1-ethyl-1H-indol-3-yl)acrylonitrile (21i). Yellow solid, 91% yield, mp 272–273 °C; ^{1}H NMR (400 MHz, DMSO-d_6) δ 12.06 (s, 1H), 8.62 (d, J = 11.4 Hz, 2H), 8.44 (s, 1H), 7.97 (d, J = 7.8 Hz, 1H), 7.76 (d, J = 2.6 Hz, 1H), 7.70 (d, J = 8.1 Hz, 1H), 7.44 (d, J = 8.8 Hz, 1H), 7.37 (t, J = 7.1 Hz, 1H), 7.30 (t, J = 7.4 Hz, 1H), 6.90 (dd, J = 8.8, 2.4 Hz, 1H), 4.44 (q, J = 7.2 Hz, 2H), 4.06 (q, J = 7.0 Hz, 2H), 1.46 (t, J = 7.2 Hz, 3H), 1.38 (t, J = 7.0 Hz, 3H); ^{13}C NMR (100 MHz, DMSO-d_6) δ 180.91, 155.29, 144.80, 136.32, 134.46, 133.33, 131.69, 128.50, 127.86, 124.00, 122.62, 121.13, 119.34, 114.63, 114.05, 113.57, 111.77, 110.10, 104.66, 102.10, 63.75, 42.17, 15.61, 15.32. HRMS (ESI) *m/z* calcd for $C_{24}H_{22}N_3O_2$: 384.1667 (M + H)$^+$, found: 384.1676.

4.1.6.10 3-(1-Ethyl-1H-indol-3-yl)-2-(5-propoxy-1H-indole-3-carbonyl)acrylonitrile (21j). Yellow solid, 93% yield, mp 294–295 °C. ^{1}H NMR (400 MHz, DMSO-d_6) δ 12.02 (s, 1H), 8.63 (s, 1H), 8.62 (s, 1H), 8.45 (s, 1H), 7.96 (d, J = 7.7 Hz, 1H), 7.78 (d, J = 2.4 Hz, 1H), 7.69 (d, J = 9.2 Hz, 1H), 7.45 (d, J = 8.8 Hz, 1H), 7.38–7.27 (m, 2H), 6.91 (dd, J = 8.8, 2.4 Hz, 1H), 4.43 (q, J = 7.2 Hz, 2H), 3.96 (t, J = 6.6 Hz, 2H), 1.77 (h, J = 7.4 Hz, 2H), 1.45 (t, J = 7.2 Hz, 3H), 1.01 (t, J = 7.4 Hz, 3H); ^{13}C NMR (100 MHz, DMSO-d_6) δ 180.90, 155.47, 144.80, 136.31, 134.38, 133.31, 131.65, 128.52, 127.86, 123.99, 122.62, 121.15, 119.30, 114.66, 114.09, 113.53, 111.75, 110.11, 104.77, 102.06, 69.83, 42.17, 22.67, 15.58, 10.94. HRMS (ESI) *m/z* calcd for $C_{25}H_{24}N_3O_2$: 398.1824 (M + H)$^+$, found: 398.1839.

4.1.6.11 3-(1-Methyl-1H-indol-3-yl)-2-(5-propoxy-1H-indole-3-carbonyl)acrylonitrile (21k). Yellow solid, 95% yield, mp 224–225 °C. ^{1}H NMR (400 MHz, DMSO-d_6) δ 8.56 (s, 1H), 8.50 (s, 1H), 8.39 (s, 1H), 7.88 (d, J = 7.7 Hz, 1H), 7.72 (d, J = 2.6 Hz, 1H), 7.59 (d, J = 8.1 Hz, 1H), 7.43 (d, J = 8.8 Hz, 1H), 7.38–7.26 (m, 2H), 6.89 (dd, J = 8.8, 2.6 Hz, 1H), 3.93 (s, 3H), 3.74 (s, 3H), 1.73 (h, J = 7.2 Hz, 2H), 0.97 (t, J = 7.4 Hz, 3H); ^{13}C NMR (100 MHz, DMSO-d_6) δ 181.11, 155.47, 145.00, 137.33, 135.06, 134.19, 131.45, 128.20, 127.69, 124.17, 122.82, 121.12, 119.02, 114.57, 113.59, 111.74, 109.85, 104.80, 101.63, 69.94, 34.20, 22.57, 10.88. HRMS (ESI) *m/z* calcd for $C_{24}H_{22}N_3O_2$: 384.1667 (M + H)$^+$, found: 384.1676.

4.1.6.12 3-(1-Ethyl-1H-indol-3-yl)-2-(5-isopropoxy-1H-indole-3-carbonyl)acrylonitrile (21l). Yellow solid, 91% yield, mp 196–

197 °C. ^{1}H NMR (400 MHz, DMSO-d_6) δ 12.00 (s, 1H), 8.64 (s, 1H), 8.61 (s, 1H), 8.45 (s, 1H), 7.97 (d, J = 7.7 Hz, 1H), 7.78 (d, J = 2.6 Hz, 1H), 7.69 (d, J = 8.1 Hz, 1H), 7.44 (d, J = 8.8 Hz, 1H), 7.39–7.27 (m, 2H), 6.89 (dd, J = 8.8, 2.4 Hz, 1H), 4.57 (quintet, J = 6.0 Hz, 1H), 4.43 (q, J = 7.2 Hz, 2H), 1.45 (t, J = 7.2 Hz, 3H), 1.31 (d, J = 6.1 Hz, 6H); ^{13}C NMR (100 MHz, DMSO-d_6) δ 180.92, 154.07, 144.83, 136.32, 134.49, 133.32, 131.77, 127.90, 123.99, 122.62, 121.15, 119.34, 115.32, 114.60, 113.56, 111.75, 110.12, 106.97, 102.08, 70.46, 42.17, 22.44, 15.59. HRMS (ESI) m/z calcd for $C_{24}H_{22}N_3O_2$: 384.1667 (M + H)$^+$, found: 384.1676.

4.1.6.13 2-(5-Isopropoxy-1H-indole-3-carbonyl)-3-(1-methyl-1H-indol-3-yl)acrylonitrile (21m). Yellow solid, 94% yield, mp 220–221 °C. ^{1}H NMR (400 MHz, DMSO-d_6) δ 12.00 (s, 1H), 8.60 (d, J = 11.1 Hz, 2H), 8.44 (s, 1H), 7.96 (d, J = 7.8 Hz, 1H), 7.78 (d, J = 2.6 Hz, 1H), 7.64 (d, J = 8.2 Hz, 1H), 7.44 (d, J = 8.7 Hz, 1H), 7.39–7.27 (m, 2H), 6.89 (dd, J = 8.7, 2.5 Hz, 1H), 4.57 (p, J = 6.1 Hz, 1H), 4.00 (s, 3H), 1.31 (d, J = 6.1 Hz, 6H). ^{13}C NMR (100 MHz, DMSO-d_6) ^{13}C NMR (101 MHz, DMSO) δ 184.84, 180.89, 154.06, 144.82, 137.34, 134.88, 134.45, 131.75, 128.32, 127.89, 124.00, 122.65, 121.11, 119.14, 115.32, 114.58, 113.57, 111.74, 109.91, 106.95, 101.91, 70.46, 34.22, 22.44, 22.40. HRMS (ESI) m/z calcd for $C_{25}H_{24}N_3O_2$: 398.1824 (M + H)$^+$, found: 398.2055.

4.1.6.14 2-(5,6-Dimethoxy-1H-indole-3-carbonyl)-3-(1-methyl-1H-indol-3-yl)acrylonitrile (21n). Yellow solid, 95% yield, mp 286–289 °C. ^{1}H NMR (400 MHz, DMSO-d_6) δ 8.60 (s, 1H), 8.56 (s, 1H), 8.33 (s, 1H), 7.93 (d, J = 7.6 Hz, 1H), 7.76 (s, 1H), 7.63 (d, J = 8.1 Hz, 1H), 7.40–7.26 (m, 2H), 7.08 (s, 1H), 3.98 (s, 3H), 3.82 (s, 3H), 3.81 (s, 3H); ^{13}C NMR (100 MHz, DMSO-d_6) δ 180.75, 147.94, 146.94, 144.73, 137.32, 134.87, 132.28, 131.06, 128.29, 124.03, 122.69, 121.18, 119.86, 119.01, 114.96, 111.71, 109.88, 103.95, 101.75, 96.05, 6.15, 34.19. HRMS (ESI) m/z calcd for $C_{23}H_{20}N_3O_3$: 386.1460 (M + H)$^+$, found: 386.1488.

4.1.6.15 2-(5,6-Dimethoxy-1H-indole-3-carbonyl)-3-(1-ethyl-1H-indol-3-yl)acrylonitrile (21o). Yellow solid, 94% yield, mp 250–251 °C. ^{1}H NMR (400 MHz, DMSO) δ 8.54 (d, J = 7.0 Hz, 2H), 8.30 (s, 1H), 7.87 (d, J = 7.7 Hz, 1H), 7.72 (s, 1H), 7.60 (d, J = 8.1 Hz, 1H), 7.35–7.24 (m, 2H), 7.07 (s, 1H), 4.33 (q, J = 7.2 Hz, 2H), 3.79 (s, 9H), 1.41 (t, J = 7.3 Hz, 3H). $\cdot$ ^{13}C NMR (100 MHz, DMSO-d_6) δ 180.84, 147.86, 146.86, 144.84, 136.24, 133.27, 132.10, 130.84, 128.40, 122.73, 121.27, 119.71, 119.09, 114.90, 111.66, 110.03, 103.78, 101.56, 95.88, 56.04, 42.18, 15.38. HRMS (ESI) m/z calcd for $C_{24}H_{22}N_3O_3$: 400.1616 (M + H)$^+$, found: 400.1651.

4.1.6.16 3-(1-(4-Chlorobenzyl)-1H-indol-3-yl)-2-(5,6-dimethoxy-1H-indole-3-carbonyl)-acrylonitrile (21p). Yellow solid, 95% yield, mp 294–295 °C. ^{1}H NMR (400 MHz, DMSO-d_6) δ 11.90 (s, 1H), 8.74 (s, 1H), 8.62 (s, 1H), 8.36 (s, 1H), 7.97 (d, J = 7.2 Hz, 1H), 7.77 (s, 1H), 7.63 (d, J = 7.7 Hz, 1H), 7.44 (d, J = 8.4 Hz, 3H), 7.32 (dd, J = 15.9, 8.3 Hz, 5H), 7.08 (s, 1H), 5.69 (s, 2H), 3.83 (s, 3H), 3.82 (s, 3H); ^{13}C NMR (100 MHz, DMSO-d_6) δ 180.73, 147.95, 146.97, 144.51, 136.51, 136.23, 133.90, 132.98, 132.58, 131.11, 129.68, 129.26, 128.57, 124.18, 122.72, 120.91, 114.90, 112.08, 110.55, 103.93, 102.96, 96.05, 56.13, 49.77. HRMS (ESI) m/z calcd for $C_{29}H_{23}ClN_3O_3$: 496.1424 (M + H)$^+$, found: 496.1405.

4.1.6.17 2-(1H-Indole-3-carbonyl)-3-(4-methoxyphenyl) acrylonitrile (21q).[37] Yellow solid, 92% yield, mp 257–259 °C (lit mp 256–258 °C). ^{1}H NMR (400 MHz, DMSO-d_6) δ 12.25 (s, 1H), 8.45 (s, 1H), 8.20 (s, 2H), 8.09 (d, J = 8.7 Hz, 2H), 7.56 (d, J = 7.7 Hz, 1H), 7.28 (s, 2H), 7.15 (d, J = 8.6 Hz, 2H), 3.87 (s, 3H); ^{13}C NMR (100 MHz, DMSO-d_6) δ 181.93, 163.21, 152.48, 137.09, 135.83, 133.33, 126.69, 125.38, 123.96, 122.79, 121.89, 118.93, 115.22, 114.20, 112.93, 108.41, 56.12.

4.1.6.18 3-(3,4-Dimethoxyphenyl)-2-(1H-indole-3-carbonyl) acrylonitrile (21r).[37] Yellow solid, 94% yield, mp 258–260 °C (lit mp 260–261 °C). ^{1}H NMR (400 MHz, DMSO-d_6) δ 12.27 (s, 1H), 8.47 (s, 1H), 8.22 (d, J = 9.5 Hz, 2H), 7.80 (s, 1H), 7.57 (d, J = 6.8 Hz, 1H), 7.32–7.24 (m, 2H), 7.15 (d, J = 8.6 Hz, 1H), 3.87 (s, 3H), 3.84 (s, 3H); ^{13}C NMR (100 MHz, DMSO-d_6) δ 181.87, 153.14, 152.88, 149.12, 137.08, 135.74, 126.74, 126.38, 125.45, 123.94, 122.76, 121.93, 119.14, 114.24, 113.20, 112.91, 112.22, 108.33, 56.26, 55.96.

4.2 Biology protocols

4.2.1 MTT assay. C4-2, PC-3, and 22Rv1 prostate cancer cells were cultured in RPMI 1640 media, while HEK293 (human kidney) and MCF7 (human breast cancer) cells were maintained in Dulbecco's modified Eagle's medium (DMEM). Both media were supplemented with 10% fetal bovine serum (FBS), 100 µg per mL streptomycin, and 100 I.U. per mL penicillin. For the MTT assay, 5000 cells per well were plated in 96-well plates. After 12 h of incubation, the cells were treated with various concentrations of **21a–r**, ranging from 0.1 µM to 40 µM. A 0.1% DMSO solution served as the vehicle control. Following 48 h of treatment, the media were removed, and the cells were washed with PBS. Then, 100 µL of serum-free media and an MTT cocktail (5 mg mL^{-1}) in a 4 : 1 ratio was added to each well. The cells were incubated for 4 h at 37 °C. Afterward, the MTT solution was aspirated, cells were washed with PBS, and 100 µL of DMSO was added to dissolve the formazan crystals. Absorbance was measured at 570 nm using a Tecan Spectrafluor Plus plate reader. Relative inhibition was calculated by dividing the mean absorbance of treated cells by the mean absorbance of DMSO-treated control cells. The IC$_{50}$ values and dose–response curves were generated through nonlinear regression analysis using the sigmoidal dose–response model with variable slope in GraphPad Prism, version 6.0 (GraphPad Software Inc., CA, USA).

4.2.2 Acridine orange/ethidium bromide assay. To investigate the effects of the **21j** on plasma membrane permeability, chromatin condensation, and nuclear morphology, AO/EB assay was performed. C4-2 cells (0.25 × 10^5) were seeded on 12 mm coverslips in 24-well plates for 12 h. The cells were subsequently treated with DMSO control or **21j** (10 and 20 µM) for 48 h. Following treatments and media removal, the cells were washed with PBS. The cells were then incubated with a mixture containing AO (100 µg mL^{-1}) and EB (100 µg mL^{-1}) in PBS for 20 min. The cells were washed with PBS and imaged using a Nikon fluorescence microscope, with green fluorescence observed using the FITC channel and red fluorescence observed using the TRITC channel.

4.2.3 JC-1 staining. To assess the impact of compound **21j** on mitochondrial health, JC-1 staining was performed. C4-2 cells (0.25 × 10^5) were seeded onto 12 mm coverslips for 12 h, following which they were exposed to DMSO or **21j** (10 or 20 µM)

for 48 h. The cells were afterwards washed with PBS and incubated with JC-1 dye (2 μM) in PBS for 20 min. Following incubation, the cells were washed, and images were captured using a Nikon fluorescence microscope with FITC (green) and TRITC (red) channels. Healthy mitochondria emit orange fluorescence in the TRITC channel due to aggregation, while depolarized mitochondria show green color due to reduced JC-1 accumulation.

4.2.4 Measurement of intracellular reactive oxygen species (ROS) levels. To assess intracellular ROS levels, the fluorogenic dye 2′,7′-dichlorofluorescein diacetate (H2DCFDA) was employed. C4-2 cells seeded on coverslips were treated with DMSO, **21j** (10 μM), or H_2O_2 (10 μM) for 48 h. Following treatment, the cells were washed with PBS and subsequently incubated with 100 μL of H2DCFDA in PBS at 2 μM final concentration for 40 min at 37 °C. Following incubation, the cells were washed with PBS, and intracellular ROS levels were visualized and imaged using the FITC channel on a Nikon inverted fluorescence microscope.

4.2.5 Western blot analysis. C4-2 cells were treated with DMSO, 20 μM of **21j**, or 100 nM of colchicine for 48 h at 37 °C. The cells were washed and lysed using a hypotonic buffer. The proteins were separated using SDS-PAGE and transferred to a polyvinylidene difluoride (PVDF) membrane. The membrane was blocked with 5% skim milk in 0.1% TBST. It was then incubated overnight at 4 °C with a tubulin primary antibody (1 : 5000 dilution), obtained from the Developmental Studies Hybridoma Bank (DSHB). Following washes with 0.1% TBST, the membrane was incubated with an HRP-conjugated secondary antibody for 1 h at room temperature. Protein bands were visualized using a chemiluminescence detection reagent (Pierce Biotechnology) and imaged with a GeneGnomeXRQ chemiluminescence imager.

4.2.6 Tubulin polymerization assay. C4-2 cells were plated for 16 h. The cells were then treated with either 10 μM of compound **21j** or 100 nM of colchicine for 48 h at 37 °C. The cells were lysed using a buffer containing 1 mM $MgCl_2$, 2 mM EGTA, 0.5% NP40, 2 mM phenylmethylsulfonyl fluoride (PMSF), and 20 mM Tris–HCl (pH 6.8). Ultracentrifugation was employed to separate the polymerized tubulin (pellet) from the depolymerized tubulin (supernatant). The pellet was resuspended in the lysis buffer, and protein concentration was determined using the Bradford assay. Equal amounts of protein from both pellet and supernatant fractions were loaded onto a 12% SDS-PAGE gel, followed by immunoblotting to detect tubulin levels in the different fractions.

4.2.7 Immunofluorescence. C4-2 cells were seeded onto coverslips for 16 h that had been coated with poly-lysine. The cells were treated with DMSO or **21j** at concentrations of 10 μM and 20 μM for 24 h. The cells were fixed, permeabilized using ice-cold methanol. To block non-specific binding, the cells were incubated for one hour with a blocking solution containing 2% BSA and 1% Triton X-100 in 1× PBS. The coverslips were incubated overnight at 4 °C with tubulin antibody, followed by FITC-conjugated goat anti-mouse secondary antibody for 3 h in the dark. The images were captured using a BZ-X810 Keyence fluorescence microscope.

4.2.8 Clonogenic assay. 1000 cells per well were plated in a 6-well plate. The plates were incubated for 10–12 days in the incubator. After incubation, cells were washed with 1× PBS and fixed with cold solution of methanol and acetic acid (3 : 1) for 5–10 min and subsequently photographed. The assay was performed in duplicates.

5. Computational methods

The detailed methodology of MD simulation study is mentioned in the ESI.†

Data availability

The authors confirm that the data supporting the findings of this study are available within the article and/or its ESI.†

Conflicts of interest

There are no conflicts to declare.

Acknowledgements

References

1 W. Yang, H. Peng, M. He, Z. Peng and G. Wang, Novel tubulin polymerization inhibitors based on the hybridization of coumarin and indole ring: Design, synthesis and bioactivities evaluation, *J. Mol. Struct.*, 2024, **1305**, 137761.

2 Y. Wan, Y. Li, C. Yan, M. Yan and Z. Tang, Indole: A privileged scaffold for the design of anti-cancer agents, *Eur. J. Med. Chem.*, 2019, **183**, 111691.

3 A. Mehra, V. Sharma, A. Verma, S. Venugopal, A. Mittal, G. Singh and B. Kaur, Indole derived anticancer agents, *ChemistrySelect*, 2022, 7, e202202361.

4 A. Carbone, M. Pennati, B. Parrino, A. Lopergolo, P. Barraja, A. Montalbano, V. Spanò, S. Sbarra, V. Doldi and M. De Cesare, Novel 1 H-pyrrolo [2, 3-b] pyridine derivative nortopsentin analogues: Synthesis and antitumor activity in peritoneal mesothelioma experimental models, *J. Med. Chem.*, 2013, **56**, 7060–7072.

5 F. Y. Miyake, K. Yakushijin and D. A. Horne, A Facile Synthesis of Dragmacidin B and 2, 5-Bis (6 '-bromo-3 '-indolyl) piperazine, *Org. Lett.*, 2000, **2**, 3185–3187.

6 A. A. Al-Karmalawy, M. Rashed, M. Sharaky, H. S. Abulkhair, M. M. Hammouda, H. O. Tawfik and M. A. Shaldam, Novel

fused imidazotriazines acting as promising top. II inhibitors and apoptotic inducers with greater selectivity against head and neck tumors: Design, synthesis, and biological assessments, *Eur. J. Med. Chem.*, 2023, **259**, 115661.

7 B. Marianna, M. Radka, K. Martin, V. Janka and M. Jan, Design, Synthesis and Antiproliferative Evaluation of Bis-Indole Derivatives with a Phenyl Linker: Focus on Autophagy, *Molecules*, 2022, **28**, 251.

8 D. Kumar, V. Arun, N. Maruthi Kumar, G. Acosta, B. Noel and K. Shah, A Facile Synthesis of Novel Bis-(indolyl)-1, 3, 4-oxadiazoles as Potent Cytotoxic Agents, *ChemMedChem*, 2012, **7**, 1915–1920.

9 B. Jiang and X.-H. Gu, Syntheses and cytotoxicity evaluation of bis (indolyl) thiazole, bis (indolyl) pyrazinone and bis (indolyl) pyrazine: Analogues of cytotoxic marine bis (indole) alkaloid, *Bioorg. Med. Chem.*, 2000, **8**, 363–371.

10 A. S. Negi, Y. Gautam, S. Alam, D. Chanda, S. Luqman, J. Sarkar, F. Khan and R. Konwar, Natural antitubulin agents: Importance of 3, 4, 5-trimethoxyphenyl fragment, *Bioorg. Med. Chem.*, 2015, **23**, 373–389.

11 P. A. Yakkala, S. Rahaman, P. L. Soukya, S. A. Begum and A. Kamal, An update on the development on tubulin inhibitors for the treatment of solid tumors, *Expert Opin. Ther. Targets*, 2024, **28**, 193–220.

12 V. K. Rao, A. Ashtam, D. Panda and S. K. Guchhait, Natural-Product-Inspired Discovery of Trimethoxyphenyl-1, 2, 4-triazolosulfonamides as Potent Tubulin Polymerization Inhibitors, *ChemMedChem*, 2024, **19**, e202300562.

13 A. Kamal, V. Srinivasulu, V. L. Nayak, M. Sathish, N. Shankaraiah, C. Bagul, N. S. Reddy, N. Rangaraj and N. Nagesh, Design and synthesis of C3-pyrazole/chalcone-linked beta-carboline hybrids: antitopoisomerase I, DNA-interactive, and apoptosis-inducing anticancer agents, *ChemMedChem*, 2014, **9**, 2084–2098.

14 A. Kamal, J. S. Reddy, M. J. Ramaiah, D. Dastagiri, E. V. Bharathi, M. V.-M. Sagar, S. N. C. V. L. Pushpavalli, P. Ray and M. Pal-Bhadra, Design, synthesis and biological evaluation of imidazopyridine/pyrimidine-chalcone derivatives as potential anticancer agents, *MedChemComm*, 2010, **5**, 355–360.

15 C. Kontogiorgis, M. Mantzanidou and D. Hadjipavlou-Litina, Chalcones and their potential role in inflammation, *Mini-Rev. Med. Chem.*, 2008, **8**, 1224–1242.

16 A. Agarwal, K. Srivastava, S. Puri and P. M. Chauhan, Synthesis of substituted indole derivatives as a new class of antimalarial agents, *Bioorg. Med. Chem. Lett.*, 2005, **15**, 3133–3136.

17 X.-F. Liu, C.-J. Zheng, L.-P. Sun, X.-K. Liu and H.-R. Piao, Synthesis of new chalcone derivatives bearing 2, 4-thiazolidinedione and benzoic acid moieties as potential anti-bacterial agents, *Eur. J. Med. Chem.*, 2011, **46**, 3469–3473.

18 N. Perin, L. Hok, A. Beč, L. Persoons, E. Vanstreels, D. Daelemans, R. Vianello and M. Hranjec, N-substituted benzimidazole acrylonitriles as *in vitro* tubulin polymerization inhibitors: Synthesis, biological activity and computational analysis, *Eur. J. Med. Chem.*, 2021, **211**, 113003.

19 Y. Ma, K. Yakushijin, F. Miyake and D. Horne, A concise synthesis of indolic enamides: Coscinamide A, coscinamide B, and igzamide, *Tetrahedron Lett.*, 2009, **50**, 4343–4345.

20 L. Gupta, A. Talwar and P. M. Chauhan, Bis and tris indole alkaloids from marine organisms: new leads for drug discovery, *Curr. Med. Chem.*, 2007, **14**, 1789–1803.

21 D. Kumar, N. M. Kumar, K. Akamatsu, E. Kusaka, H. Harada and T. Ito, Synthesis and biological evaluation of indolyl chalcones as antitumor agents, *Bioorg. Med. Chem. Lett.*, 2010, **20**, 3916–3919.

22 (a) A. Boumendjel, X. Ronot and J. Boutonnat, Chalcones derivatives acting as cell cycle blockers: potential anti cancer drugs?, *Curr. Drug Targets*, 2009, **10**, 363–371; (b) J. Yan, J. Chen, S. Zhang, J. Hu, L. Huang and X. Li, Synthesis, Evaluation, and Mechanism Study of Novel Indole-Chalcone Derivatives Exerting Effective Antitumor Activity Through Microtubule Destabilization in Vitro and in Vivo, *J. Med. Chem.*, 2016, **59**, 5264–5283.

23 D. Kumar, N. M. Kumar, S. Ghosh and K. Shah, Novel bis (indolyl) hydrazide–hydrazones as potent cytotoxic agents, *Bioorg. Med. Chem. Lett.*, 2012, **22**, 212–215.

24 (a) X. Liu, J. Jin, Y. Wu, B. Du, L. Zhang, D. Lu, Y. Liu, X. Chen, J. Lin and H. Chen, Fluoroindole chalcone analogues targeting the colchicine binding site of tubulin for colorectal oncotherapy, *Eur. J. Med. Chem.*, 2023, **257**, 115540; (b) M. Hawash, D. C. Kahraman, A. Olgac, S. G. Ergun, E. Hamel, R. Cetin-Atalay and S. N. Batyas, Design and synthesis of novel substituted indole-acrylamide derivatives and evaluation of their anti-cancer activity as potential tubulin-targeting agents, *J. Mol. Struct.*, 2022, **1254**, 132345.

25 F. F. Fleming, L. Yao, P. Ravikumar, L. Funk and B. C. Shook, Nitrile-containing pharmaceuticals: efficacious roles of the nitrile pharmacophore, *J. Med. Chem.*, 2010, **53**, 7902–7917.

26 (a) L. Guan, H. Yang, Y. Cai, L. Sun, P. Di, W. Li, G. Liu and Y. Tang, ADMET-score–a comprehensive scoring function for evaluation of chemical drug-likeness, *Medchemcomm*, 2019, **10**, 148–157; (b) M. Venkatanarayana and P.-K. Dubey, Simple and efficient Knoevenagel synthesis of (E)-2-((1H-indol-3-yl) methylene)-3-oxoindolylnitrile catalysed by PPh_3, *J. Chem. Sci.*, 2011, **123**, 609–614; (c) M. Tarleton, L. Dyson, J. Gilbert, J.-A. Sakoff and A.-M. Cluskey, Focused library development of 2-phenylacrylamides as broad spectrum cytotoxic agents, *Bioorg. Med. Chem.*, 2013, **21**, 333–347; (d) D. Kumar, N.-M. Kumar, M.-P. Tantak, M. Ogura, E. Kusaka and T. Ito, Synthesis and identification of α-cyano bis (indolyl) chalcones as novel anticancer agents, *Bioorg. Med. Chem. Lett.*, 2014, **24**, 5170–5174.

27 D. Kumar, N. M. Kumar, K.-H. Chang, R. Gupta and K. Shah, Synthesis and in-vitro anticancer activity of 3, 5-bis (indolyl)-1, 2, 4-thiadiazoles, *Bioorg. Med. Chem. Lett.*, 2011, **21**, 5897–5900.

28 F. Riu, L. Sanna, R. Ibba, S. Piras, V. Bordoni, M. A. Scorciapino, M. Lai, S. Sestito, L. Bagella and A. Carta, A comprehensive assessment of a new series of 5′, 6′-difluorobenzotriazole-acrylonitrile derivatives as microtubule targeting agents (MTAs), *Eur. J. Med. Chem.*, 2021, **222**, 113590.

29 (*a*) J. Slaett, I. Romero and J. Bergman, Cyanoacetylation of indoles, pyrroles and aromatic amines with the combination cyanoacetic acid and acetic anhydride, *Synthesis*, 2004, 2760–2765; (*b*) A. Daina, O. Michielin and V. Zoete, SwissADME: a free web tool to evaluate pharmacokinetics, drug-likeness and medicinal chemistry friedliness of small molecules, *Sci. Rep.*, 2017, **7**, 42712.

30 O. Ursu, A. Rayan, A. Goldblum and T. I. Oprea, Understanding drug-likeness, *Wiley Interdiscip. Rev.:Comput. Mol. Sci.*, 2011, **1**, 760–781.

31 C. A. Lipinski, F. Lombardo, B. W. Dominy and P. J. Feeney, Experimental and computational approaches to estimate solubility and permeability in drug discovery and development settings, *Adv. Drug Delivery Rev.*, 1997, **23**, 3–25.

32 S. M. Huang, J. M. Strong, L. Zhang, K. S. Reynolds, S. Nallani, R. Temple, S. Abraham, S. A. Habet, R. K. Baweja and G. J. Burckart, New era in drug interaction evaluation: US Food and Drug Administration update on CYP enzymes, transporters, and the guidance process, *J. Clin. Pharmacol.*, 2008, **48**, 662–670.

33 A. Olyaei and M. Sadeghpour, Chemistry of 3-cyanoacetyl indoles: synthesis, reactions and applications: a recent update, *RSC Adv.*, 2023, **13**, 21710–21745.

34 L. De Luca, S. De Grazia, S. Ferro, R. Gitto, F. Christ, Z. Debyser and A. Chimirri, HIV-1 integrase strand-transfer inhibitors: design, synthesis and molecular modeling investigation, *Eur. J. Med. Chem.*, 2011, **46**, 756–764.

35 S. Vogel, D. Kaufmann, M. Pojarová, C. Müller, T. Pfaller, S. Kühne, P. J. Bednarski and E. V. Angerer, Aroyl hydrazones of 2-phenylindole-3-carbaldehydes as novel antimitotic agents, *Bioorg. Med. Chem.*, 2008, **16**, 6436–6447.

36 Q. Wu, Y. Luo, A. Lei and J. You, Aerobic copper-promoted radical-type cleavage of coordinated cyanide anion: nitrogen transfer to aldehydes to form nitriles, *J. Am. Chem. Soc.*, 2016, **138**, 2885–2888.

37 T. Mark, L. Dyson, J. A. Gilbert and A. McCluskey, Focused library development of 2-phenylacrylamides as broad spectrum cytotoxic agents s, *Bioorg. Med. Chem.*, 2013, **21**, 333–347.